Supplementary Methods

Salt flux synthesis

Single crystals of pyrite (FeS_2) in equilibrium with gold were prepared using an $AlCl_3$/KCl flux and a permanent temperature gradient (Chareev, 2016; Chareev et al., 2016). Starting chemicals were: pre-synthesized FeS_2 powder, crystalline S, Au wire Ø 0.5 mm, reagent grade KCl, and anhydrous aluminum chloride $AlCl_3$ (Fluka, 98%). The pyrite powder, a few pieces of S, and Au wire were loaded into a silica glass ampoule (8 mm ID, 12 mm OD, 110 mm length). Then, hygroscopic $AlCl_3$ was promptly weighed in the air and immediately loaded into the ampoule. Potassium chloride taken in the mass ratio $AlCl_3$:KCl = 1.5:1 was added to the ampoule. Finally, the ampoule was evacuated down to a 10^{-4} bar pressure and sealed. The sealed ampoule was loaded into a horizontal tube furnace, heated to the synthesis temperature in 1-2 hours and kept at this temperature for 30 days. The temperature of the hot and cold part of the ampoule was 620 °C and ~ 550 °C respectively. At the end of the experiment, the ampoule was extracted from the furnace and cooled on air. The cold part of the ampoule with crystals of pyrite, Au, and S, was cut off, and Al-K chlorides were dissolved in distilled water. The crystals of pyrite were rinsed two times in alcohol and two - three times in acetone in an ultrasonic bath. The rinsed crystals have been dried in a muffle furnace at 70 ºC for a few minutes.

For an arsenopyrite (FeAsS) synthesis the carbonyl Fe powder, crystalline S and As, Au foil, KCl, NaCl, CsCl, KBr, and KI (all reagent grade) were used. In some cases powders of FeAsS, FeAs, AsS, As_2S_3, FeS, and FeS_2, synthesized at 400 - 600 ºC by conventional solid-state synthesis (Clark, 1960), were used as precursors for the synthesis of the Au-bearing arsenopyrite. The As/S ratio in the charging material was kept close to equimolar by a combination of Fe + As + S, FeAs + S, Fe + AsS, FeS + As, or $Fe_1As_1S_1$ + small amount of Fe, or As, or S. Two series of synthesis experiments were performed. In the first series, the mixture of CsCl/NaCl/KCl (30 at.% NaCl/24.5

at.% KCl) with melting temperature of 478ºC (Fullam, 1971) was used as a salt flux. In the second series, chlorides of Na and K were replaced by NaBr and KI, respectively (every load contained NaCl + KI or NaBr + KCl). The temperature of the hot part of the ampoule was 580 °C, of the cold part - ~ 520 °C. The concentration of the "invisible" Au was nearly the same in the crystals of both series, despite the fact that the crystal sizes of the second series were bigger than those of the first series. The synthesis procedure was similar to the one described for pyrite. Crystals of arsenopyrite and aggregates of arsenopyrite-pyrrhothite crystals were obtained. Only pure arsenopyrite was used for XAFS experiments.

For the synthesis of löllingite ($FeAs_2$) the powders of $FeAs_2$ and As were used as the initial substances and a CsCl/NaCl/KCl mixture was used as a flux. The temperature of the hot part of the ampoule was 650 °C, of the cold part - ~ 570 °C. The synthesis procedure was similar to the one described above for pyrite and arsenopyrite.

The XRD pattern of synthesized phases corresponded to pure pyrite PDF#42-1340, arsenopyrite PDF#65-2304, and löllingite PDF#65-3795.

Hydrothermal synthesis

Hydrothermal experiments were carried out at 450 °C and 1 kbar pressure using Ti autoclaves (VT-8 alloy) with an internal volume of ~25 ml. An initial reagent (FeS powder synthesized by conventional solid-state technique) was placed into small Ti container attached to the Ti partition in the upper part of the autoclave. A strip of Au foil was also attached to the partition, avoiding contact with FeS. The autoclaves were loaded with the necessary amount of $S_{(cr)}$ (taking into account the reaction of S with FeS with the formation of pyrite), distilled water degassed by boiling, and Ar saturated. In one experiment, 0.5*m* H_2SO_4 solution was used in order to create more oxidizing conditions. Pressure in the autoclaves was controlled by the degree of filling

with the experimental solution. The closed autoclaves were placed into the gradient less furnaces preheated to 450 °C. The duration of the experiments was 3 weeks. The autoclaves were quenched in cold water. In these experiments a powder of Au-bearing pyrite was obtained. The grain size of the synthesized Au-bearing pyrite was n·10 μm, and the XRD pattern corresponded to pure pyrite PDF#42-1340.

Synthesis of model compounds

The method of the Au_2S synthesis is described in Tagirov et al. (2006). The same batch of Au_2S was used in the present study. Powders of $AuSb_2$ and Au_2Bi were synthesized from pure elements. Weighted stoichiometric amounts of Au, Sb and Bi (~0.5 g for each phase) were hermetically sealed in evacuated silica glass ampoules. The ampoules were slowly heated up to a temperature of 550 °C ($AuSb_2$) and 700 °C (Au_2Bi) to melt the mixture of initial reagents, and then quenched in cold water. Then the reacted mixture was annealed at 350C °C ($AuSb_2$) and 300 °C (Au_2Bi) for 30 days. After the annealing the ampoule with $AuSb_2$ was slowly cooled to room temperature, whereas the ampoule with Au_2Bi was quenched in cold water. The produced mixtures were ground in an agate mortar under acetone, and sealed in new ampoules. Then the annealing procedure was repeated. The nature of the obtained materials was verified by means of powder XRD.

Analytical methods

The morphology and composition of the synthesized minerals was studied using scanning electron microscopy (SEM), electron probe micro-analysis (EPMA), laser ablation inductively

coupled mass spectrometry (LA-ICP-MS), and wet chemistry (only for the hydrothermal pyrites). Details of these methods are described in Tagirov et al. (2016) and, therefore, will be only briefly outlined here. The JSM-5610LV microscope equipped with INCA-450 energy dispersive spectrometer was used to study the grains morphology. The EPMA analyses were performed using a JEOL JXA-8200 WD/ED combined electron probe microanalyzer equipped with 5 wavelength dispersive X-ray spectrometers. The concentration of Au was determined using LiF crystal, the limits of detection (2σ) for Au was 0.01 wt% at 100 nA beam current. The concentration of ^{197}Au isotope was determined using LA-ICP-MS in polished sections of pyrite and arsenopyrite grains (New Wave 213 laser, and Thermo X Series2 quadrupole ICP-MS). The sulfide reference material MASS-1 (Wilson et al., 2012), and in-house pyrrhotite $Fe_{0.9}S$ (18 ppm Au, synthesized using Wohlgemuth-Ueberwasser et al. (2007) method and calibrated with respect to the concentration of Au against standards prepared by J.H.G. Laflamme and A. Peregoedova at the Université Quiébec à Chicoutimi), were used as the calibration standards. The ^{57}Fe isotope was used as an internal standard. The total Au content in hydrothermal pyrites was determined by ICP-MS after the decomposition of samples in aqua regia and sorption of Au on the POLYORGS resin.

Calculation of sulfur fugacity

In the hydrothermal experiments on synthesis of pyrite sulfur fugacity $f(S_{2(g)})$ was controlled by the elemental sulfur dissolution and hydrolysis reactions,

$$S_{(l)} = S^{\circ}_{(aq)} \qquad (S1)$$

$$3S^{\circ}_{(aq)} + 2H_2O = 2H_2S_{(aq)} + SO_{2(aq)} \qquad (S2)$$

$$H_2S_{(aq)} + 2H_2O = SO_{2(aq)} + 3H_{2(g)} \qquad (S3)$$

$2SO_{2(aq)} + 4H_{2(g)} = S_{2(g)} + 4H_2O$ (S4)

The method of $f(S_{2(g)})$ calculation is similar to the one used in Tagirov et al. (2016). The calculation was performed using an HCh software package (Shvarov, 2008). The activity coefficients of charged aqueous species were calculated using the modified Debye-Hückel equation, the ion size parameter a was taken to be 4.5 Å for all species. Thermodynamic properties for aqueous species (including HSO_4^-, SO_4^{2-}, SO_2, HSO_3^-, SO_3^{2-}, $H_2S_2O_4$, $HS_2O_4^-$, $S_2O_4^{2-}$, H_2S, HS^-, H^+ and OH^-) were taken from the SUPCRT92 database (Johnson et al., 1992). Sulfur and $S_{2(g)}$ thermodynamic data from Naumov et al. (1971) and Robie and Hemingway (1995) were used, correspondingly.

X-ray absorption spectroscopy (XAS)

XAS spectra of Au-bearing pyrite, arsenopyrite, löllingite, and other substances (Au foil and synthetic Au_2S, $AuSb_2$ and Au_2Bi) were collected at high-brilliance X-ray absorption and X-ray emission spectroscopy undulator beamline ID26 (Gauthier et al., 1999) of the European Synchrotron Radiation Facility (ESRF) at Grenoble. The incident energy was selected using the <111> reflection from a double Si crystal monochromator. The rejection of higher harmonics was achieved by three Cr/Pd mirrors positioned at an angle of 2.5 mrad relative to the incident beam. The flux of the incident X-ray beam was approximately $2 \cdot 10^{13}$ photon s^{-1} on the sample position. XANES spectra were simultaneously measured in the total fluorescence yield (TFY) mode using a photodiode and in the high energy resolution fluorescence detection (HERFD) mode using an X-ray emission spectrometer (Glatzel and Bergmann, 2005; Kvashnina and Scheinost, 2016). The sample, analyzer crystal, and photon detector (silicon drift diode) were arranged in a vertical Rowland geometry. The Au XANES/EXAFS HERFD spectra at the L_3 edge were obtained by recording the intensity of the Au $L\alpha_1$ emission line (9713 eV) as a function of the incident energy. The emission

energy was selected using the <660> reflection of four spherically bent Ge crystal analyzers (1 m curvature radius) aligned at 80° Bragg angle. A combined (incident convoluted with emitted) energy resolution of 1.2 eV was determined by measuring the elastic peak. The intensity was normalized to the incident flux.

For the heating experiment, a powder of hydrothermal pyrite was loaded into a silica glass capillary (Polymicro Technologies™, 350 μm OD, 200 μm ID, 20 mm length) together with a small amount of sulfur, which prevented sample oxidation and fixed sulfur fugacity $f(S_2)$ during the experiment. The capillary was evacuated and hermetically sealed. This simple experimental technique was developed by Chou et al. (2008, 2012) and Ding (2010) for the Raman spectroscopy of solids and liquids, and we adopted it for the synchrotron experiment. For *in situ* XAS measurements, the capillaries were placed into a microtomography furnace (Bellet et al., 2003). Temperature was measured by a K-type thermocouple in contact with the capillary at an accuracy of ±5 °C.

Density Functional Theory (DFT) calculations

The QUANTUM ESPRESSO software package (Giannozzi et al., 2009) was used for quantum chemical DFT calculations. We employed a projector-augmented wave (PAW) all-electron description of electron-ion-core interactions (Blöhl, 1994; Kresse, 1999) and the Perdew-Burke-Ernzerhof (PBE) exchange-correlation functional. For the electronic structure calculations, the self-consistent field (SCF) method was applied with a 100 Ry kinetic energy cutoff for the plane waves, a 1500 Ry charge density cutoff, and an SCF tolerance better than 10^{-9}. The relaxation of atomic positions and cell parameters was performed in a supercell containing 2×2×2 unit cells for the pyrite and arsenopyrite, and 2×2×3 unit cells for the löllingite. The crystal structure and supercell parameters were optimized using the BFGS algorithm for atomic coordinates with a convergence

threshold of 10^{-3} Ry/au for forces and 10^{-4} Ry for energy. Topological atomic charges were determined from the quantum theory of atoms in molecules (QTAIM). The local atomic charges were calculated by integrating the charge density within Bader volumes around the atoms (Otero-de-la-Roza et al., 2009, 2014).

EXAFS spectra analysis

The analysis of EXAFS spectra provided insight into the Au local atomic environment. The EXAFS data ($\chi_{exp}(k)$) were analyzed using the IFEFFIT software package (Ravel and Newville, 2005). After the standard procedures of pre-edge subtraction and spline background removal, interatomic distances (R_i), coordination numbers (N_i), and Debye–Waller factors (σ^2) were determined by the non-linear fitting of experimental data with the theoretical spectrum described by the equation

$$\chi(k) = S_0^2 \sum_{i=1}^{n} \frac{N_i F_i(k)}{R_i^2 k} e^{\frac{-2R_i}{\lambda(k)}} e^{-2\sigma_i^2 k^2} \sin\left(2kR_i + \varphi_i(k)\right) \quad . \quad (1)$$

The parameters necessary for the simulation of the theoretical spectra (photoelectron mean free path $\lambda(k)$, amplitude $F_i(k)$, phase shift $\varphi_i(k)$) were calculated *ab initio* using the FEFF6 program (Zabinsky et al., 1995). The statistical uncertainty of the calculation method is 0.01–0.02 Å for refined R_i in the first coordination shell.

XANES spectra simulation

Theoretical calculations of Au L_3 edge XANES spectra were performed using two approaches: finite difference method (FDM) and full multiple scattering (FMS). The FDM is implemented in the FDMNES code (Joly, 2001; Guda et al., 2015). Relativistic self-consistent field FDMNES calculations were carried out with the exchange-correlation part of the potential in a local

density approximation (Hedin and Lundqvist, 1971). The final electronic states were calculated in a full core hole screening. Atomic clusters inside the spheres with radii of 8 Å and 7 Å were chosen for self-consistent calculations and FDM XANES calculations, respectively. To account for many body effects and core hole lifetime broadening, the arctangent convolution was applied (Bunău and Joly, 2009). Although the FDMNES procedure is computationally expensive, it is best for systems with non-spherical charge distribution.

The FMS spectra modeling was performed using the FEFF9.6 revision 4 code (Rehr et al., 2010), which is based on the self-consistent muffin-tin potentials. The Dirac-Hara exchange-correlation potentials were used. The parameter for the imaginary potential was set to -2 to account for the reduced broadening of HERFD-XANES spectra. Self-consistent calculations were refined with a radius of 6 Å around the central Au atom, whereas a radius of 7 Å was chosen for FMS calculations. The RPA core hole approximation was applied to simulate the central excited atom.

References Cited for Supplementary Methods

Akinfiev, N.N., and Zotov, A.V. (2010) Thermodynamic description of aqueous species in the system Cu-Ag-Au-S-O-H at temperatures of 0-600°C and pressures of 1-3000 bar. Geochemistry International, 48, 714-720.

Bellet, D., Gorges, B., Dallery, A., Bernard, P., Pereiro, E., and Baruchel, J. (2003) A 1300 K furnace for in situ X-ray microtomography. Journal of Applied Crystallography, 36, 366-367.

Blöhl, P.E. (1994) Projector augmented-wave method. Physical Review B, 50, 17953–17979.

Bunău O., and Joly Y. (2009) Self-consistent aspects of x-ray absorption calculations. Journal of Physics: Condensed Matter, 21, 345501.

Chareev, D.A. (2016). General principles of the synthesis of chalcogenides and pnictides in salt melts using a steady-state temperature gradient. Crystallography Reports, 61(3), 506-511.

Chareev, D.A., Volkova, O.S., Geringer, N.V., Koshelev, A.V., Nekrasov, A.N., Osadchii, V.O., ... and Filimonova, O.N. (2016). Synthesis of chalcogenide and pnictide crystals in salt melts using a steady-state temperature gradient. Crystallography Reports, 61(4), 682-691.

Chou, I-M. (2012) Optical cells with fused silica windows for the study of geological fluids. In J. Dubessy, M.-C. Gaumont and F. Rull Eds., Applications of Raman Spectroscopy to Earth Sciences and Cultural Heritage, p. 227-248. EMU Notes in Mineralogy, V. 12, London.

Chou, I-M., Song, Y., and Burruss, R.C. (2008) A new method for synthesizing fluid inclusions in fused silica capillaries containing organic and inorganic material. Geochimica et Cosmochimica Acta, 72, 5217-5231.

Clark, L.A. (1960). The Fe-As-S system - Phase relations and applications. Economic Geology, 55, 1345-1381.

Ding, J. (2010) The pH determination of palaeofluids: experimental and thermodynamic approach, 173 p. PhD thesis, Université Henri Poincaré, Nancy.

Fullam, H.T. (1971) Physical property measurements on cesium chloride and cesium chloride – alkali metal chloride systems. 52 p. Atlantic Richfield Hanford Company.

Gauthier, C., Sole, V.A., Signorato, R., Goulon, J., and Moguiline, E. (1999) The ESRF beamline ID26: X-ray absorption on ultra dilute sample. Journal of Synchrotron Radiation, 6, 164-166.

Giannozzi, P., Baroni, S., Bonini, N., Calandra, M., Car, R., Cavazzoni, C., Ceresoli, D., Chiarotti, G.L., Cococcioni, M., Dabo, I. and others (2009) QUANTUM ESPRESSO: a modular and open-source software project for quantum simulations of materials. Journal of Physics: Condensed Matter, 21, 395502.

Glatzel, P., and Bergman, U. (2005) High resolution 1s core hole X-ray spectroscopy in 3d transition metal complexes - electronic and structural information. Coordination Chemistry Reviews, 249, 65-95.

Guda, S.A., Guda, A.A., Soldatov, M.A., Lomachenko, K. A., Bugaev, A. L., Lamberti, C., Gawelda, W., Bressler, C., Smolentsev, G., Soldatov, A.V., and Joly, Y. (2015) Optimized finite difference method for the full-potential XANES simulations: application to molecular adsorption geometries in MOFs and metal-ligand intersystem crossing transients. Journal of Chemical Theory and Computation, 11, 4512-4521.

Hedin, L., and Lundqvist, B. (1971) Explicit local exchange-correlation potentials. Journal of Physics C: Solid State Physics, 4, 2064–2083.

Johnson, J.W., Oelkers, E.H., and Helgeson, H.C. (1992) SUPCRT92: A software package for calculating the standard molal thermodynamic properties of minerals, gases, aqueous

species, and the reactions from 1 to 5000 bars and 0° to 1000°C. Computational Geosciences, 18, 899-947 (the updates are available at http://geopig.asu.edu/tools).

Joly, Y. (2001). X-ray absorption near-edge structure calculations beyond the muffin-tin approximation. Physical Review B, 63, 125120-125129.

Kresse, G. (1999). From ultrasoft pseudopotentials to the projector augmented-wave method. Physical Review B, 59, 1758–1775.

Kvashnina, K.O., and Scheinost, A.C. (2016) A Johann-type X-ray emission spectrometer at the Rossendirf Beamline. Journal of Synchrotron Radiation, 23, 836–841.

Longerich, H.P., Jackson, S.E., and Günther, D. (1996) Laser ablation inductively coupled plasma mass spectrometric transient signal data acquisition and analyte concentration calculation. Journal of Analytical Atomic Spectrometry, 11, 899-904.

Naumov, G.B., Ryzhenko, B.N., and Khodakovsky, I.L. (1974) Handbook of thermodynamic data. US Geologiccal Survey, Menlo Park, California.

Otero-de-la-Roza, A., Blanco, M.A., Martín Pendás, A., and Luaña, V. (2009) Critic: a new program for the topological analysis of solid-state electron densities. Computer Physics Communications, 180, 157–166.

Otero-de-la-Roza, A., Johnson, E.R., and Luaña, V. (2014) Critic2: A program for real-space analysis of quantum chemical interactions in solids. Computer Physics Communications, 185, 1007–1018.

Ravel, B., and Newville, M. (2005) ATHENA, ARTEMIS, HEPHAESTUS: data analysis for X-ray absorption spectroscopy using IFEFFIT. Journal of Synchrotron Radiation, 12, 537-541.

Rehr, J.J., Kas, J.J., Vila, F.D., Prange, M.P., and Jorissen, K. (2010). Parameter-free calculations of X-ray spectra with FEFF9. Physical Chemistry Chemical Physics, 12, 5503-5513.

Robie, R.A., and Hemingway, B.S. (1995) Thermodynamic properties of minerals and related substances at 298.15 K and 1 bar (10^5 Pascals) pressure and at higher temperatures. U.S. Geological Survey Bulletin 2131, U.S. Government Printing Office, Washington.

Shvarov, Yu.V. (2008) HCh: New potentialities for the thermodynamic simulation of geochemical systems offered by Windows. Geochemistry International, 46, 834–839.

Tagirov, B.R., Baranova, N.N., Zotov, A.V., Schott, J., and Bannykh, L.N. (2006) Experimental determination of the stabilities of $Au_2S_{(cr)}$ at 25°C and $Au(HS)_2^-$ at 25-250°C. Geochimica et Cosmochimica Acta, 70, 3689–3701.

Tagirov, B.R., Trigub, A.L., Kvashnina, K.O., Shiryaev, A.A., Chareev, D.A., Nickolsky, M.S., Abramova, V.D., and Kovalchuk, E.V. (2016) Covellite CuS as a matrix for "invisible" gold: X-ray spectroscopic study of the chemical state of Cu and Au in synthetic minerals. Geochimica et Cosmochimica Acta, 191, 58-69.

Wilson, S.A., Ridley, W.I., and Koenig, A.E. (2002) Development of sulfide calibration standards for the laser ablation inductively-coupled plasma mass spectrometry. Journal of Analytical Atomic Spectrometry, 17, 406-409.

Wohlgemuth-Ueberwasser, C.C., Ballhaus, C., Berndt, J., Stotter née Paliulionyte, V., and Meisel, T. (2007) Synthesis of PGE sulfide standards for laser ablation inductively coupled plasma mass spectrometry (LA-ICP-MS). Contributions to Mineralogy and Petrology, 154, 607-617.

Zabinsky, S.I., Rehr, J.J., Ankudinov, A., Albers, R.C., and Eller, M.J. (1995) Multiple-scattering calculations of X-ray-absorption spectra. Physical Review B, 52, 2995-3009.

Supplementary Tables

Table S1. Composition of the experimental system, aqueous solubility of $Au_{(cr)}$, and the concentration of Au in pyrite (experimental parameters t = 450 °C, P = 1 kbar).

Aut. №	Loaded into the autoclave		Au in fluid, mol kg^{-1} H_2O		$\log f(S_{2\,(g)})$, bar	Au in pyrite, ppm
	m(S)	$m(H_2SO_4)$	Experiment	Calculation[1]		
6-8	0.3	0	6.8E-07	3.4E-6	-2.8	62
6-10	0.5	0	1.4E-06	5.5E-6	-2.4	84
6-12	0.75	0	2.6E-06	8.2E-6	-2.0	78
6-13	1	0	3.7E-06	1.1E-5	-1.8	86
6-14	1.5	0	5.9E-06	1.6E-5	-1.4	86
6-16	0.5	0.5	9.3E-08	4.2E-6	-2.3	36

[1] thermodynamic data for Au aqueous species are adopted from Akinfiev and Zotov (2010).

Table S2. Concentrations of Au and Pt (ppm) in pyrite grain (salt flux synthesis, 620 °C), determined by LA-ICP-MS.

Analysis No.	Concentration	^{194}Pt	^{195}Pt	^{197}Au
Point 1	Average	2.1	2.1	70.4
	$\sigma^{(1)}$	2.4	2.1	36.4
	DL$^{(2)}$	0.00	0.00	0.02
Point 2	Average	< DL	< DL	0.6
	$\sigma^{(1)}$	0.3	0.2	0.7
	DL$^{(2)}$	0.00	0.00	0.00
Point 3	Average	0.6	0.5	0.6
	$\sigma^{(1)}$	0.9	0.9	1.1
	DL$^{(2)}$	0.00	0.00	0.01
Point 4, meas. 1	Average	0.2	0.1	399
	$\sigma^{(1)}$	0.5	0.5	223
	DL$^{(2)}$	0.00	0.00	0.03
Point 4, meas. 2	Average	0.2	0.2	5.2
	$\sigma^{(1)}$	0.6	0.5	11.7
	DL$^{(2)}$	0.00	0.00	0.03
Point 5	Average	7.3	7.2	29
	$\sigma^{(1)}$	4.3	4.4	11
	DL$^{(2)}$	0.00	0.00	0.02
Point 6	Average	< DL	< DL	< DL
	$\sigma^{(1)}$	0.6	0.6	0.3
	DL$^{(2)}$	0.00	0.00	0.03
Point 7	Average	< DL	< DL	0.0
	$\sigma^{(1)}$	0.1	0.1	0.1
	DL$^{(2)}$	0.0	0.0	0.011
Point 8	Average	0.3	0.2	1.8
	$\sigma^{(1)}$	0.6	0.6	1.6
	DL$^{(2)}$	0.00	0.00	0.00
Point 9	Average	2.5	2.3	< DL
	$\sigma^{(1)}$	2.1	1.9	0.0
	DL$^{(2)}$	0.00	0.00	0.00
Point 10	Average	2.4	2.6	< DL
	$\sigma^{(1)}$	2.1	2.3	0.2
	DL$^{(2)}$	0.00	0.00	0.00
Point 11	Average	0.8	0.9	4.0
	$\sigma^{(1)}$	1.4	1.4	3.9
	DL$^{(2)}$	0.00	0.00	0.01
Point 12	Average	2.3	2.2	9.7
	$\sigma^{(1)}$	2.2	2.2	4.6
	DL$^{(2)}$	0.00	0.00	0.01

Point 13	Average	0.3	0.3	2.1
	$\sigma^{(1)}$	0.8	0.7	2.5
	$DL^{(2)}$	0.00	0.00	0.01
Line 1	Average	1.9	1.8	< DL
	$\sigma^{(1)}$	2.2	2.0	0.4
	$DL^{(2)}$	0.1	0.1	0.01
Line 2, meas. 1	Average	0.4	0.3	1.3
	$\sigma^{(1)}$	3.7	3.6	1.7
	$DL^{(2)}$	0.0	0.0	0.02
Line 2, meas. 2	Average	4.9	4.8	135.0
	$\sigma^{(1)}$	4.2	4.1	68.5
	$DL^{(2)}$	0.0	0.0	0.02
Line 3	Average	3.9	3.5	1.6
	$\sigma^{(1)}$	4.0	4.4	1.6
	$DL^{(2)}$	0.0	0.0	0.01

(1) standard deviation;
(2) detection limit DL is calculated for each measurement in accord with Longerich et al. (1996).

Table S3. Calculated Bader atomic partial charges for pure and Au-bearing pyrite, löllingite, arsenopyrite, and for $Au_2S_{(cr)}$. Charges of atoms in covellite CuS (Tagirov et al., 2016) are given for comparison.

Au	Fe	As	S
$FeAs_2$			
	+0.16	-0.08	
FeAsS			
	+0.42	+0.18	-0.6
FeS_2			
	+0.70		-0.35
Au in $FeAs_2$ (nearest atoms to Au)			
-0.37	+0.18	-0.08; -0.01	
Au in FeAsS (nearest atoms to Au)			
-0.01	+0.43	+0.30	-0.56
Au in FeS_2 (nearest atoms to Au)			
+0.42	+0.72		-0.36
Au in Au_2S[1]			
+0.21			-0.42
Au	Cu		S
CuS			
	+0.56, +0.50		-0.84, -0.82(S_2)
Au in CuS (nearest atoms to Au)			
+0.19	+0.56, +0.48		-0.69, -0.80(S_2)

[1] calculated for Au_2S structure relaxed with DFT method, optimized lattice constant a = 5.35 Å, Au-S distance R = 2.32 Å.

Supplementary Figures

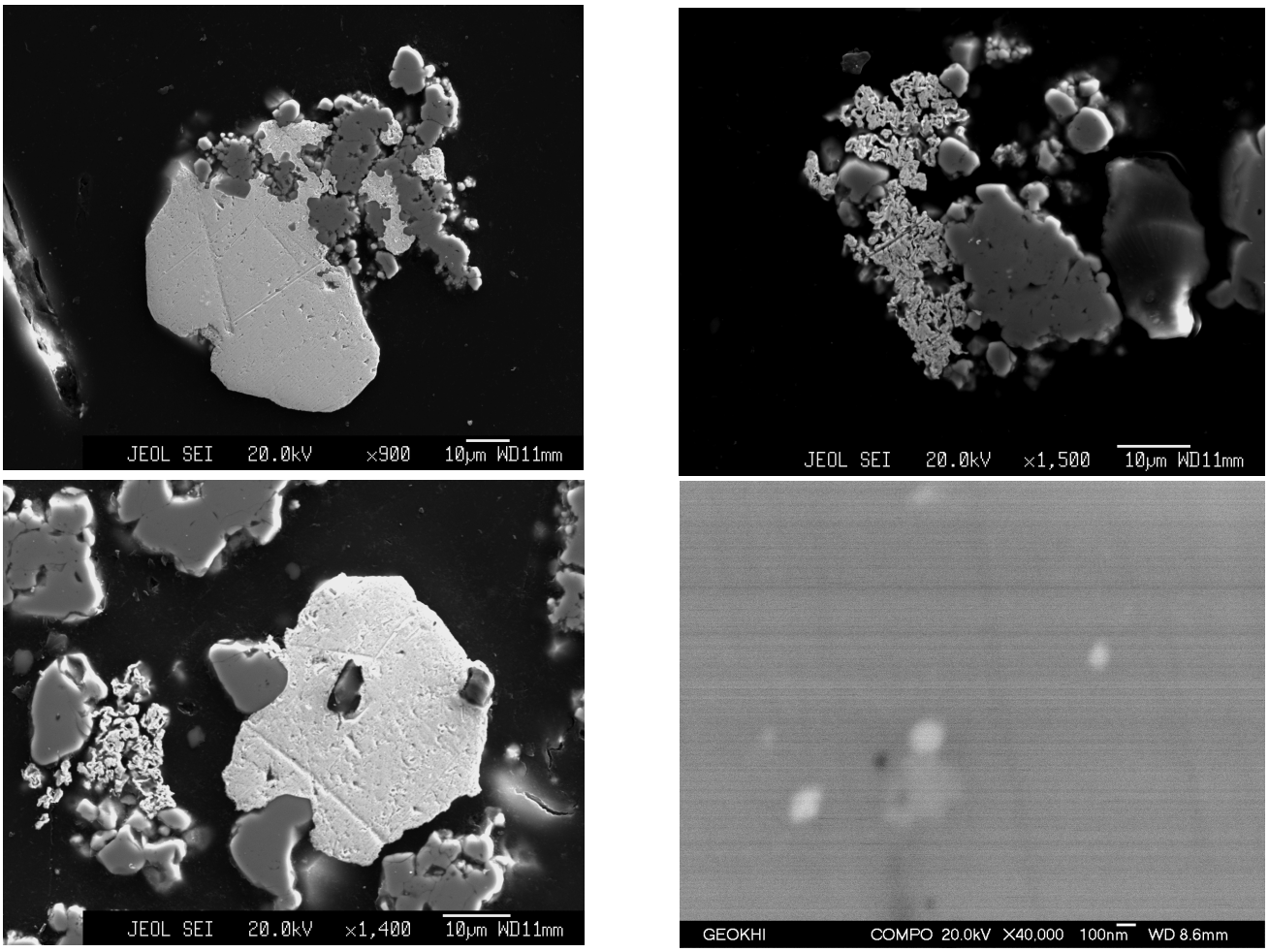

Figure S1. BSE images of the aggregates of hydrothermal pyrite + $Au_{(cr)}$. Synthesis was performed at 450 °C, 1 kbar. Experimental system composition: 0.75*m* NaOH/1*m* S, the concentration of Au dissolved in hydrothermal fluid $C(Au) = 0.07m$ (AAS analysis), calculated $pH_{T,P} = 7.3$. The light-grey nodes in the high-resolution image (*right bottom*) are probably the particles of Au metal.

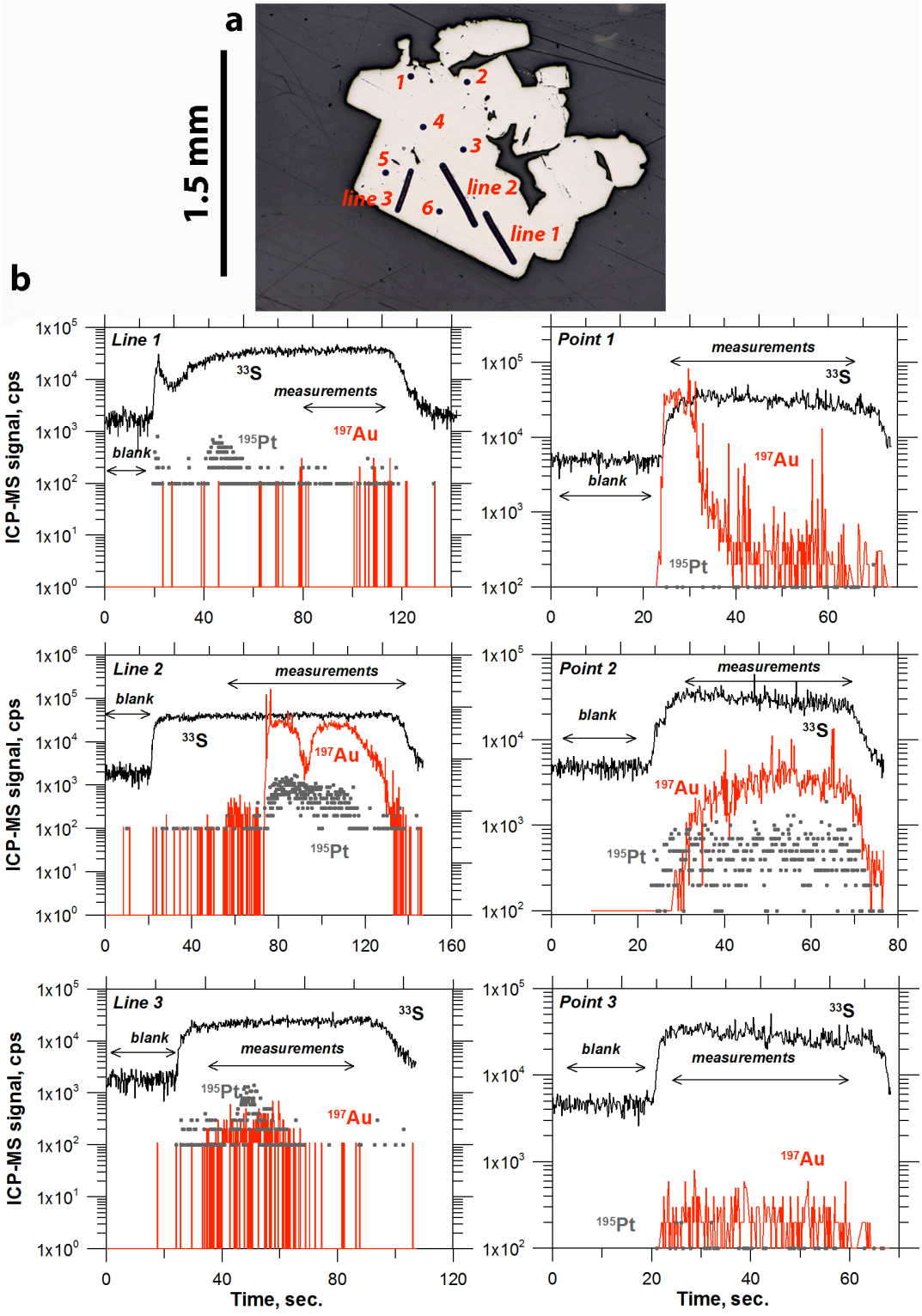

Figure S2. The concentration of Au in pyrite grain, sample CD-624 (salt-flux synthesis, t = 620 °C(hot end)/550 °C (cold end), $AlCl_3$/KCl eutectic mixture). **A.** Image of a pyrite grain after laser ablation (optical microscope); **b.** Time-resolved LA-ICP-MS spectra for trace elements. Concentrations are listed in the Table S2.

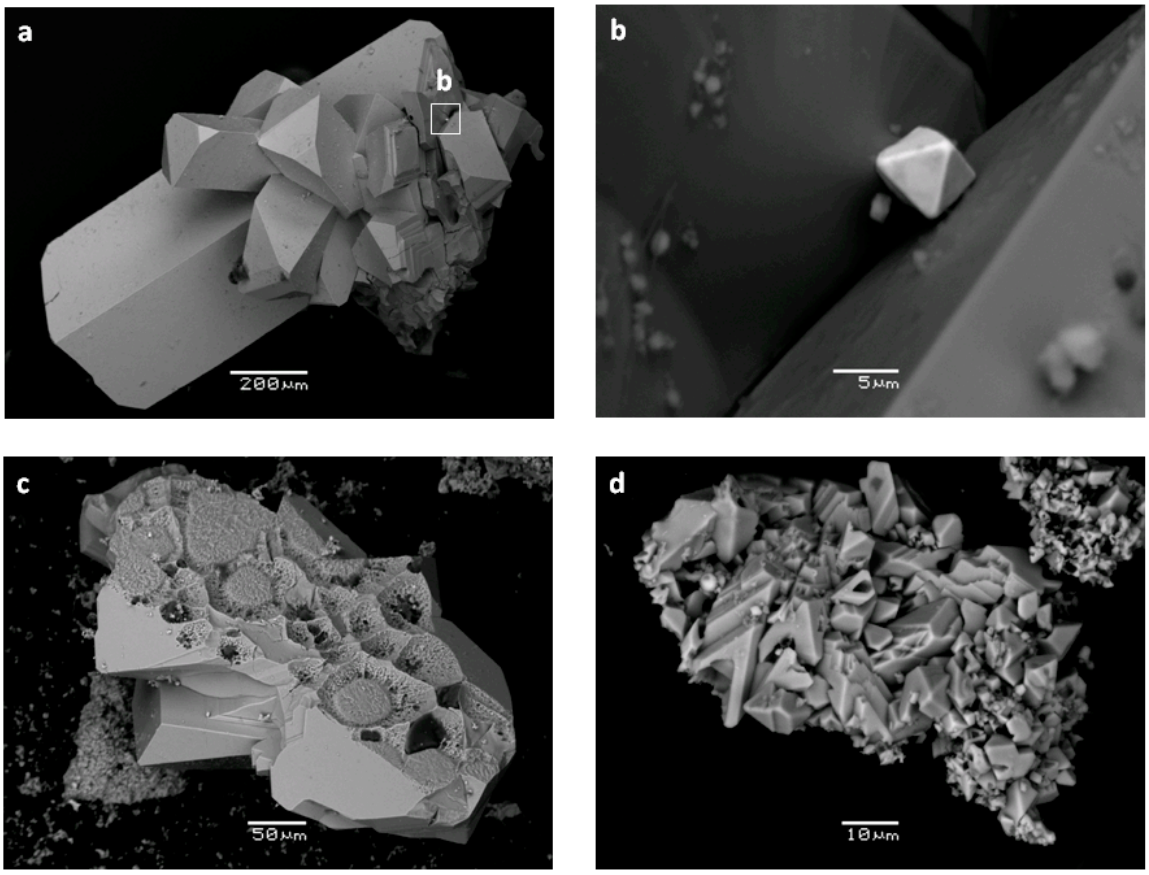

Figure S3. BSE images of the aggregates of synthetic arsenopyrite grains. Salt flux synthesis, 580 °C (hot end)/520 °C (cold end), CsCl/NaCl/KCl eutectic mixture. Figure **b** shows a grain of Au which was deposited on the surface of arsenopyrite during the experiment. Sample 5140 (figures **c** and **d**, $Fe_{0.923}As_{0.98}S$, *C*(Au) = 23±14 ppm) contains mostly chemically bound Au and was used for the XAS experiment.

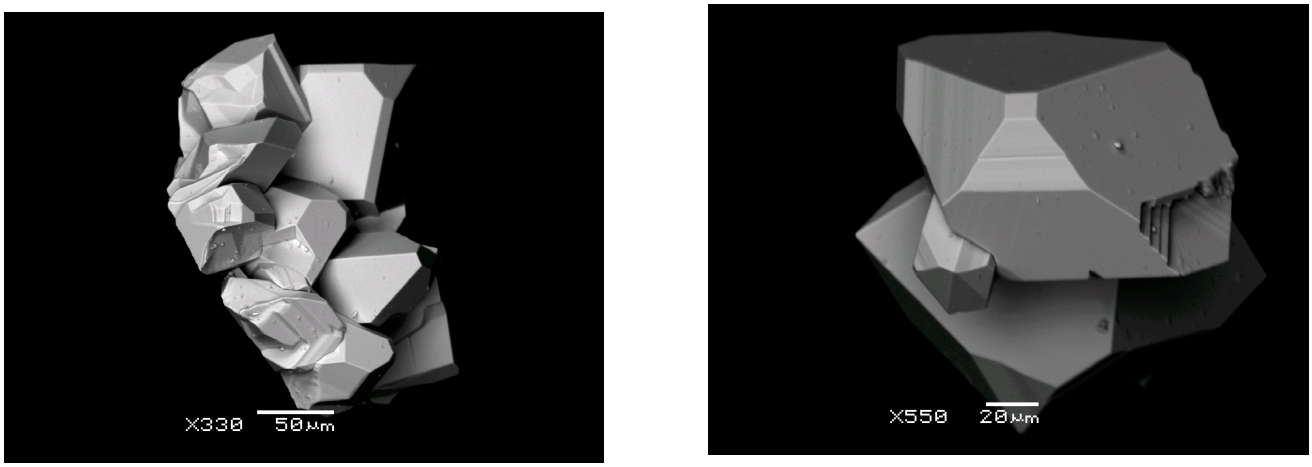

Figure S4. BSE images of the aggregates of synthetic löllingite $FeAs_2$ crystals used for XAS experiment. Salt flux synthesis, 650 °C (hot end)/570 °C (cold end), CsCl/NaCl/KCl eutectic mixture. Sample 5333, *C*(Au) = 800±300 ppm.

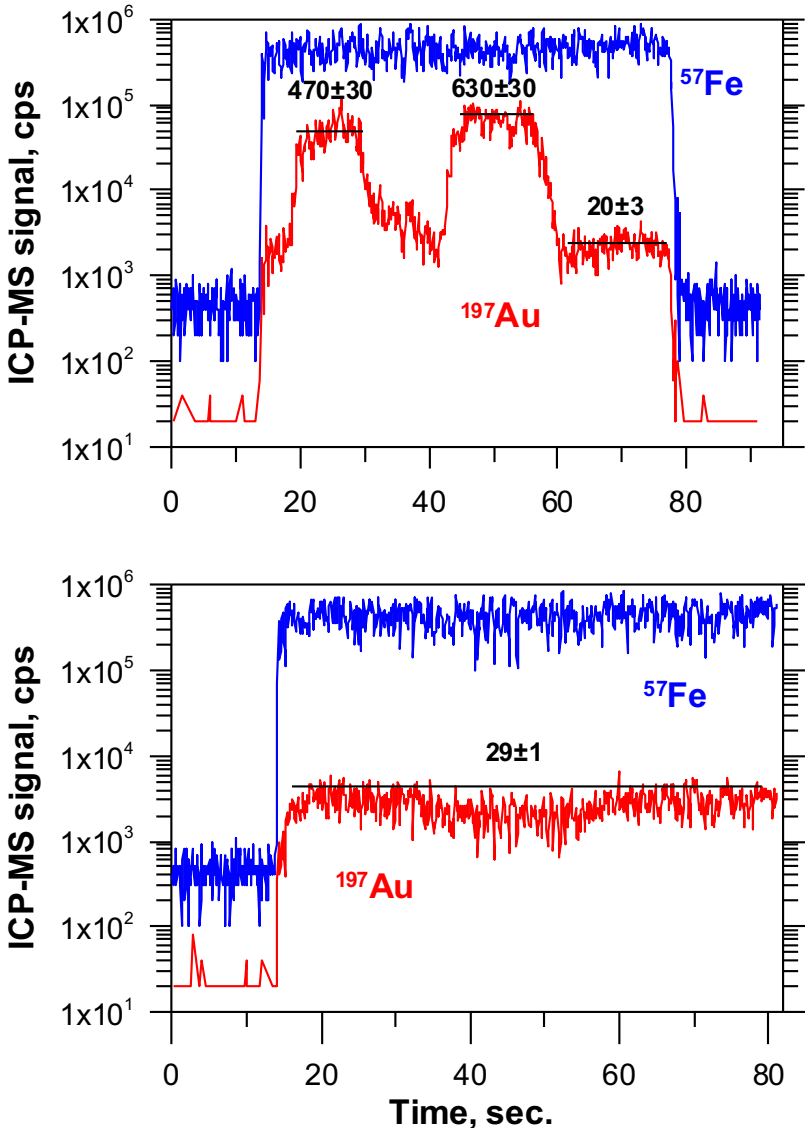

Figure S5. Time-resolved spectra for Au and Fe, expressed as counts per second for a LA-ICP-MS scans (lines) burned in an arsenopyrite grain of sample 5140. Average Au concentration (ppm) is given by numbers.

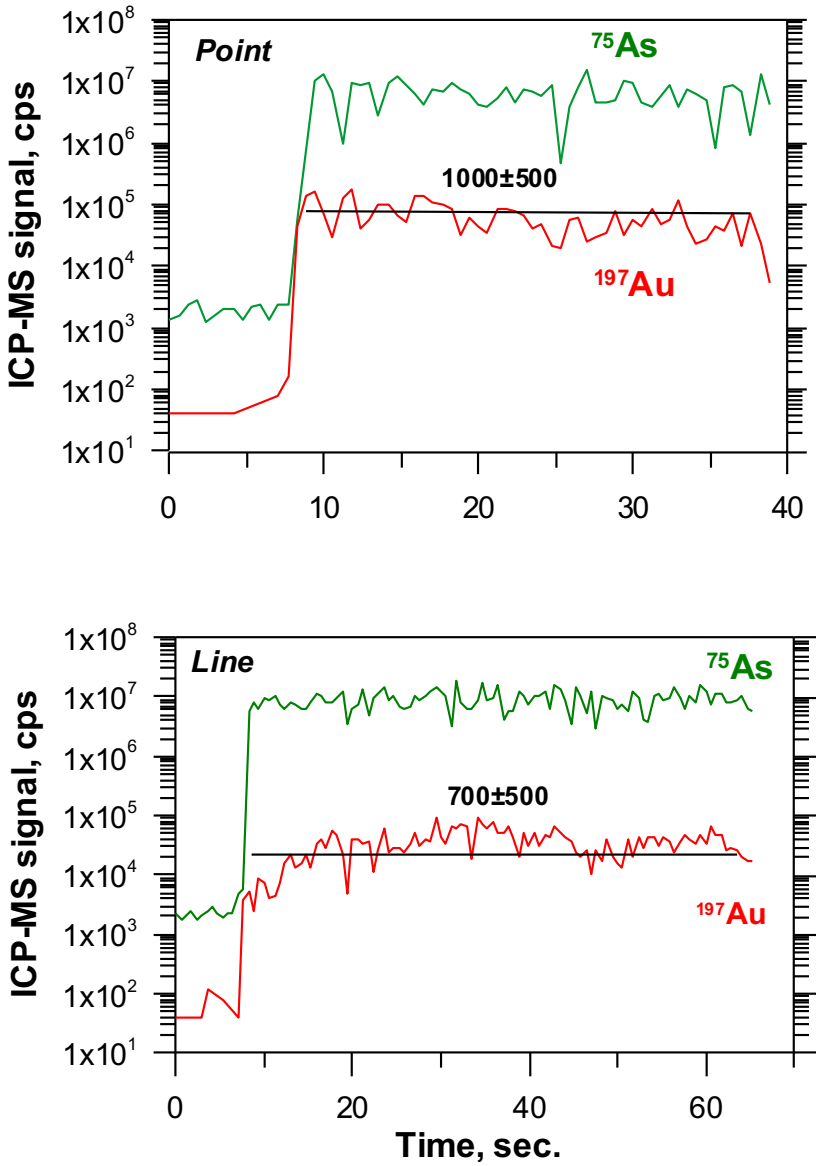

Figure S6. An example of the time-resolved spectra for Au and As, expressed as counts per second for a LA-ICP-MS scans (point and line) burned in the löllingite grains of sample 5333. Average Au concentration (ppm) is given by numbers.

Supplementary Structures: some minerals in the Fe-As-S system

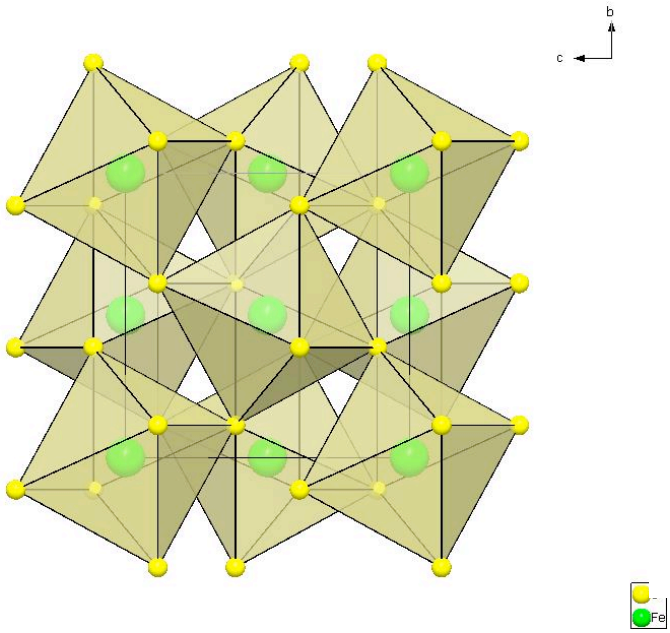

Pyrite FeS_2

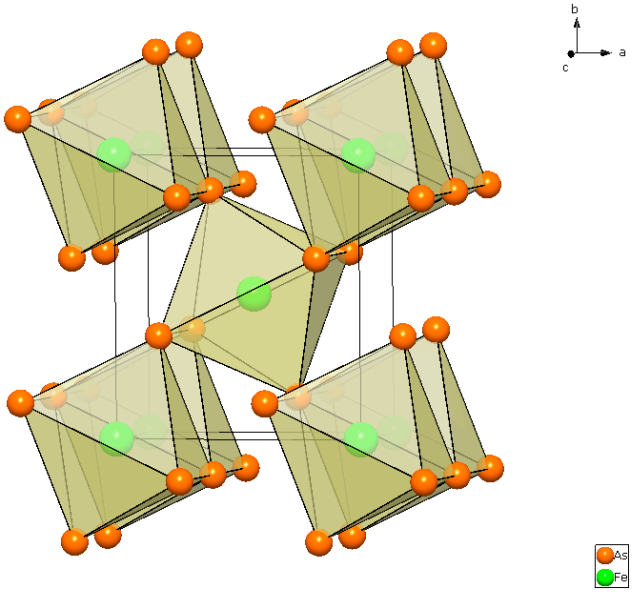

Löllingite $FeAs_2$

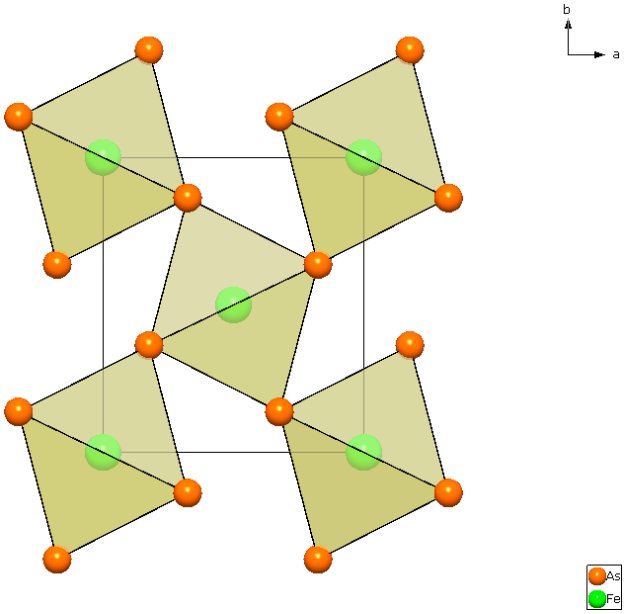

Löllingite – along *c*

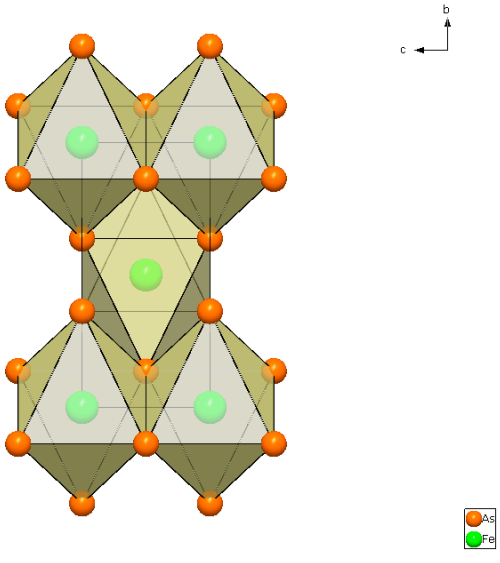

Löllingite – along a

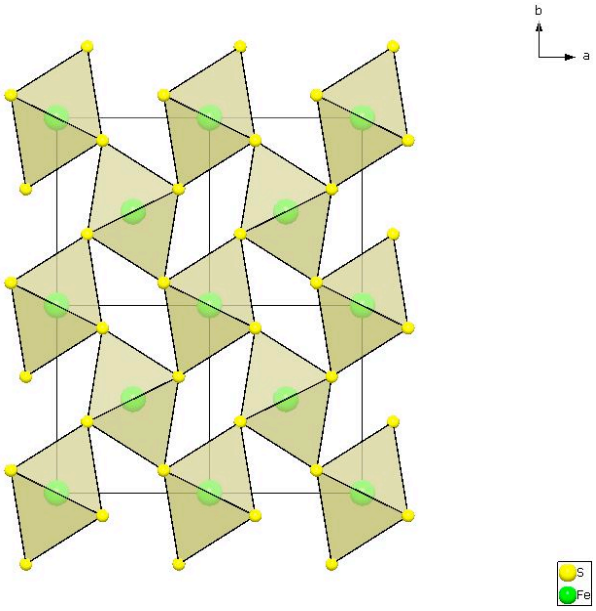

Marcasite FeS_2 (isostructural with arsenopyrite)

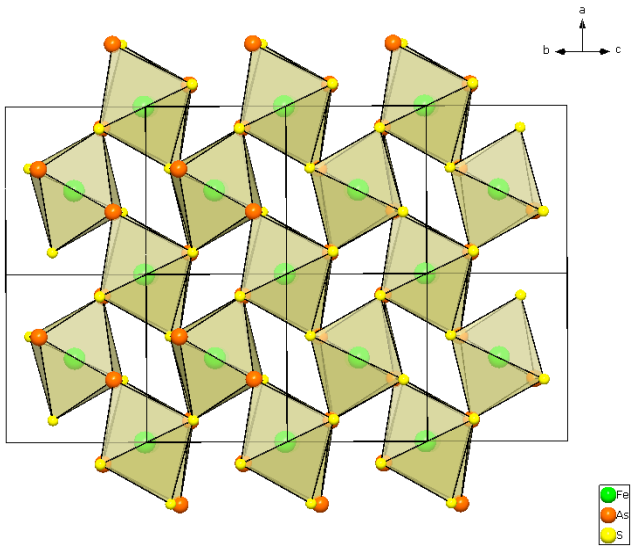

Arsenopyrite FeAsS

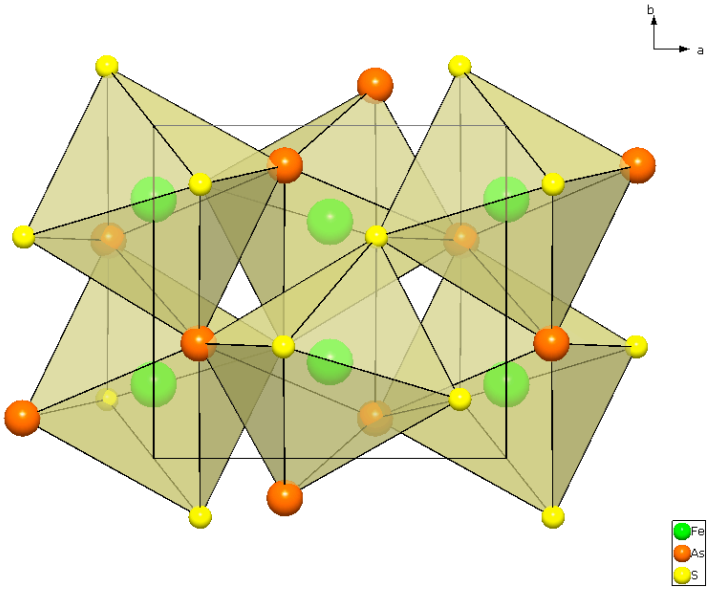

Arsenopyrite – along *c*

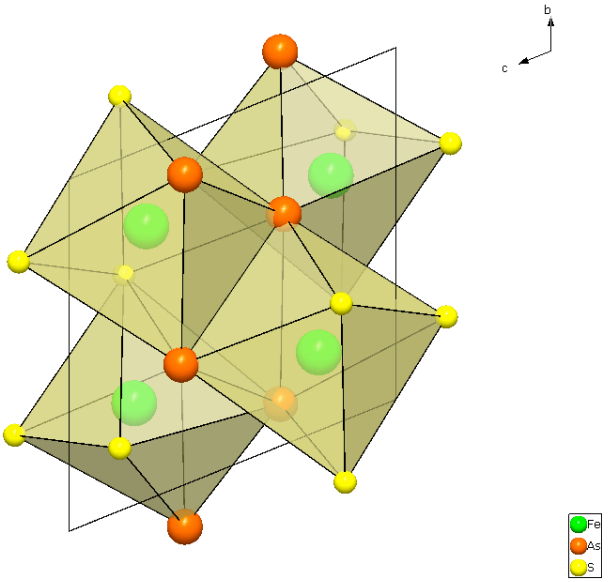

Arsenopyrite – along a